AGU100 ADVANCING EARTH AND SPACE SCIENCE

Geophysical Research Letters

RESEARCH LETTER
10.1029/2018GL080691

Special Section:
Bridging Weather and Climate: Subseasonal-to-Seasonal (S2S) Prediction

Key Points:
- A statistical approach explores the sudden warming predictability beyond the 10-day limit of dynamical forecasts
- The approach utilizes upward wave activity and meridional potential vorticity gradient to determine conditional sudden warming probabilities
- The conditional probabilities show significant information gain over climatology out to one season

Correspondence to:
M. Jucker,
publications@martinjucker.com

Citation:
Jucker, M., & Reichler, T. (2018). Dynamical precursors for statistical prediction of stratospheric sudden warming events. *Geophysical Research Letters*, *45*. https://doi.org/10.1029/2018GL080691

Received 27 SEP 2018
Accepted 8 NOV 2018
Accepted article online 19 NOV 2018

Dynamical Precursors for Statistical Prediction of Stratospheric Sudden Warming Events

M. Jucker[1,2] and T. Reichler[3]

[1]School of Earth Sciences and ARC Centre of Excellence for Climate System Science, The University of Melbourne, Melbourne, Victoria, Australia, [2]Climate Change Research Centre, University of New South Wales, Sydney, New South Wales, Australia, [3]Department of Atmospheric Sciences, University of Utah, Salt Lake City, UT, USA

Abstract This work explores dynamical arguments for statistical prediction of stratospheric sudden warming events (SSWs). Based on climate model output, it focuses on two predictors, upward wave activity in the lower stratosphere and meridional potential vorticity gradient in the upper stratosphere, and detects large values of these predictors. Then it quantifies how many SSWs are preceded by predictor events and, inversely, how many events are followed by SSWs. This allows to compute conditional probabilities of future SSW occurrence. It is found that upward wave activity leads to important increases in SSW probability within the following 3 weeks but is less important thereafter. A weak potential vorticity gradient is associated with increased SSW probability at short lags and, perhaps more importantly, decreased SSW probability at long lags. Finally, when both predictors are considered in combination, the information gain is large on the weekly and small but significant on the intraseasonal time scale.

Plain Language Summary After a breakdown of the polar vortex in the winter hemisphere stratosphere, Northern Hemisphere weather can be unusual for several months or even weeks. Therefore, there is great interest in being able to predict these breakdowns, which are known as stratospheric sudden warming events. The traditional way of forecasting these events is to run full climate models forward in time similar to everyday weather forecasting. However, this is computationally expensive and model skill is very low beyond about 2 weeks. This study explores a new, probabilistic way of prediction based on dynamical arguments. It uses the past evolution of the stratosphere to construct probabilities of occurrence as a function of lead time. It shows that meaningful information can be obtained for an entire extended winter season, which is an order of magnitude longer than traditional model forecasting.

1. Introduction

Stratospheric sudden warming events (SSWs) have been a focus of research on stratosphere-troposphere coupling for a while now. Eliassen-Palm (EP) fluxes of planetary scale can propagate from the troposphere into the stratosphere in Northern Hemisphere winter, when midlatitude to high-latitude zonal winds are westerly throughout the stratosphere (and not too strong; Charney & Drazin, 1961; Dickinson, 1969). Breaking of those waves and the associated EP flux divergence can lead to the breakdown of the stratospheric polar vortex (Holton, 1974; Matsuno, 1971; McIntyre, 1982), causing SSWs which in turn can influence the state of the troposphere on the seasonal time scale (e.g., Baldwin & Dunkerton, 2001; Scaife et al., 2017; Shaw et al., 2014; Sigmond et al., 2013). Thus, enhanced upward EP fluxes play an important role in the evolution of sudden warmings (e.g., Ayarzagüena et al., 2011; Limpasuvan et al., 2004; Matsuno, 1971; Nishii et al., 2009; Polvani & Waugh, 2004; Schneidereit et al., 2017) and peak about a week before the onset date (Charlton & Polvani, 2007; Dunn-Sigouin & Shaw, 2015; Garfinkel et al., 2010; Jucker, 2016; Martineau & Son, 2015; Nakagawa & Yamazaki, 2006).

However, various authors also note that enhanced EP flux might not be as important as previously thought. Although probably *necessary* (see below), it may not provide a *sufficient* condition for the occurrence of a sudden warming (Albers & Birner, 2014; Birner & Albers, 2017; Esler & Matthewman, 2011; Jucker, 2016; Matthewman & Esler, 2011; Scott & Polvani, 2004, 2006). Indeed, while easterly zonal momentum is required to reverse the polar vortex, its deposition also has to be at the right place. Following linear wave propagation theory, EP fluxes are directed toward higher refractive index (Karoly & Hoskins, 1982; Palmer, 1981). The only term within the refractive index depending on the dynamical background state of the atmosphere is proportional to the meridional potential vorticity gradient (henceforth *PV gradient*) q_ϕ (Matsuno, 1970). The PV gradient is proportional to second derivatives of zonal wind (equation (1)) and therefore sensitive to small wind perturbations. As a result, even weak forcing can change the refractive index substantially and hence may alter the wave propagation and divergence (Butchart et al., 1982). Previous work (e.g., Albers & Birner, 2014; Jucker, 2016) has shown that the PV gradient sharpens along the vortex edge long before anomalous upward EP flux peaks, also known as *preconditioning* (Bancalá et al., 2012; Labitzke, 1977, 1981; McIntyre, 1982; Schoeberl, 1978). The long lead time between the vortex sharpening and the onset of sudden warmings suggests that the stratospheric PV gradient could be a useful predictor for SSWs.

Therefore, this work will study the potential for improved statistical prediction of SSWs based on the pre-SSW evolution of EP flux and PV gradient, the two main quantities determining when, how much, and where in the stratosphere easterly momentum is deposited. We will make use of general circulation model data for meaningful statistical analyses, as observational and/or reanalysis data contain too few SSWs.

In section 2, we describe the general circulation model setup and derived variables to be used for the study. Section 3 validates the model and quantifies the relationship between precursors and SSWs. Section 4 examines the conditional SSW probabilities before concluding remarks in section 5.

2. Data and Methods

We use a nearly 10,000-year long control integration with a stratosphere-resolving version of the CM2.1 model from the Geophysical Fluid Dynamics Laboratory, described in Horan and Reichler (2017). These authors showed that the stratospheric dynamics of this model compare well to reanalysis in terms of SSW frequency, seasonal evolution of the polar vortex strength, and its variability. Multiple lines of work have also shown that CM2.1 simulates a very reasonable tropospheric climate (e.g., Reichler & Kim, 2008). We apply the Charlton and Polvani (2007) definition of major SSWs. Explicitly, we require a reversal of the zonally averaged zonal wind at 60°N and 10 hPa, with a return to westerly winds for at least 10 consecutive days during the same season. Also, two zero crossings have to be separated by at least 20 days to be counted as distinct events.

We detect SSWs from December to March, leading to a mean frequency of 5.9 SSWs per decade, in accordance with most other studies (Butler et al., 2015; Charlton et al., 2007; Palmeiro et al., 2015). We are not including November as we consider conditions up to 90 days before any particular SSW and want to minimize the number of summer days included in our analysis.

We compute the meridional gradient of PV (Matsuno, 1970) in the form given by Simpson et al. (2009),

$$q_\phi = \int_{\phi_0}^{\phi_1} \mathrm{d}\phi \left\{ 2\Omega\cos\phi - \left[\frac{(\bar{u}\cos\phi)_\phi}{a\cos\phi}\right]_\phi + \frac{af^2}{R_d}\left(\frac{p\theta}{T}\frac{\bar{u}_p}{\bar{\theta}_p}\right)_p \right\} \Bigg/ \int_{\phi_0}^{\phi_1} \cos\phi \mathrm{d}\phi, \tag{1}$$

where standard notation is used. Overbar $(\bar{\cdot})$ denotes zonal mean, and subscripts represent derivatives. We compute the meridional mean value between $\phi_0 = 55°$N and $\phi_1 = 75°$N and at 30 hPa, as this is where the signal in q_ϕ is strongest.

The vertical component of the quasi-geostrophic EP flux (Eliassen & Palm, 1961) is calculated following Andrews et al. (1987)

$$F_p = a\cos\phi f \frac{\overline{v'\theta'}}{\theta_p}, \tag{2}$$

where primes denote zonal asymmetries. We will only be interested in the hemispherically averaged EP fluxes at 100 hPa, defined as

$$F_z = -\int_{\phi_2}^{\phi_3} F_p \mathrm{d}\phi \Bigg/ \int_{\phi_2}^{\phi_3} \cos\phi \mathrm{d}\phi, \tag{3}$$

where the average goes from $\phi_2 = 20°$N to $\phi_3 = 90°$N, and the minus sign was added to ensure that positive F_z means upward propagation. We standardize both variables relative to the day of the year by first removing the daily climatological mean and then dividing by the daily standard deviation.

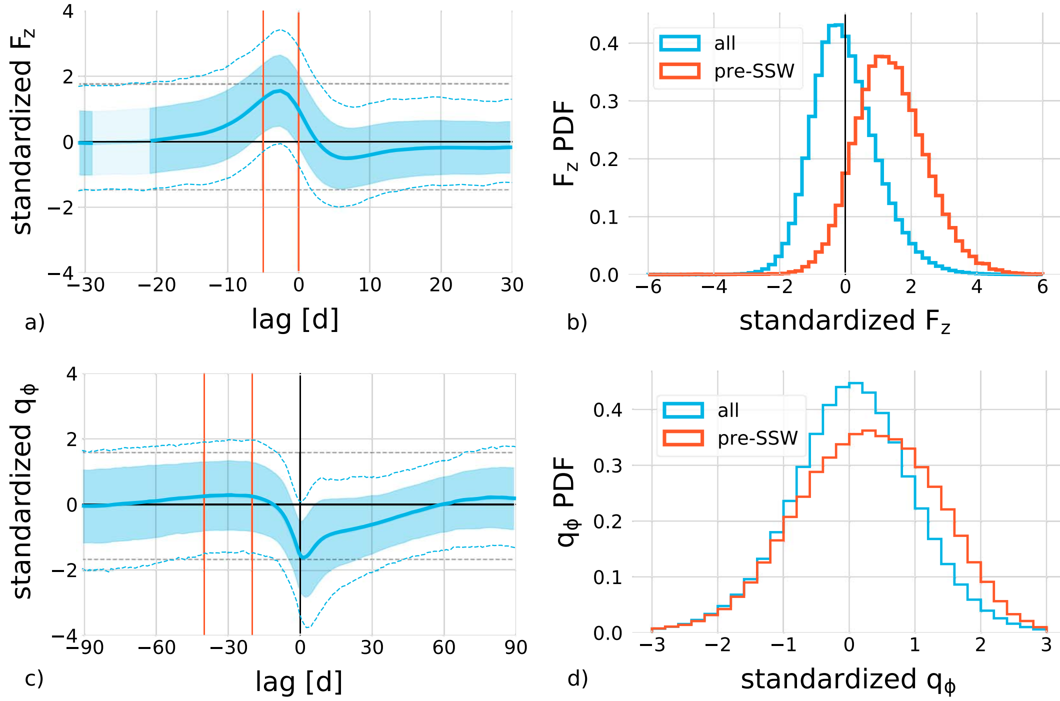

Figure 1. (left) SSW composites (onset at lag 0) of (a) upward Eliassen-Palm flux at 100 hPa and (c) meridional potential vorticity gradient at 30 hPa. The blue shading shows the range of one standard deviation around the mean and is transparent where the composite does not differ significantly in both mean and standard deviation from the entire time series (10,000-member bootstrap plus Kolmogorov-Smirnov test). The dashed blue lines show the 5th and 95th percentiles of the composites, whereas the horizontal dashed gray lines show the 5th and 95th percentiles of the entire data set. (right) Histograms of the same quantities (b, d), for all days (blue) and days associated with SSWs at lags denoted by the vertical red lines in the left panels (red). SSW = stratospheric sudden warming event; PDF = Probability Distribution Function.

We define an event E as the crossing of a given threshold of one or more variables. Any consecutive days where the variables are beyond the threshold are considered to be part of the same event.

Then, the conditional probabilities are computed by counting the number of relevant events in the model simulations:

$$P(SSW|E)(l) = \frac{\#\text{events } E \text{ at lag } l \text{ of a SSW}}{\#\text{ of events } E}, \tag{4}$$

The climatological event and SSW probabilities are

$$\overline{P(X)} = \frac{\#X \text{ in data}}{(\#\text{days in extended winter period}) \cdot (\#\text{years})}, \tag{5}$$

where X is any event, including SSWs. The empirically derived climatological SSW probability is $\overline{P(SSW)} = 0.49\%$.

We will compare the conditional probabilities (4) to the climatological probability $\overline{P(SSW)}$ (5) to estimate the impact of event E onto the probability of SSW occurrence. We note that by comparing $P(SSW|E)$ to $\overline{P(SSW)}$ we assume for the latter that all days are independent and have the same (climatological) probability of SSW occurrence. Of course, this is an approximation, as for example, the probability of occurrence of an SSW is 0 directly after an SSW, violating the assumption of independence. However, we will show a posteriori that the approximation is reasonable, as $P(SSW|E)$ converges toward $\overline{P(SSW)}$ at long lags. We expect that any event E becomes independent from SSWs at sufficiently large lags n, that is, $P(SSW|E) \xrightarrow{n \gg 1} P(SSW)$, and we verify in Figure 3 that $P(SSW) \approx \overline{P(SSW)}$ which validates our approximation.

In addition, we compute the fraction of SSWs preceded by event E within n days (Figure 2) and compare this to the empirical probability of event E during the same n days. Keeping with the above notation of X as a

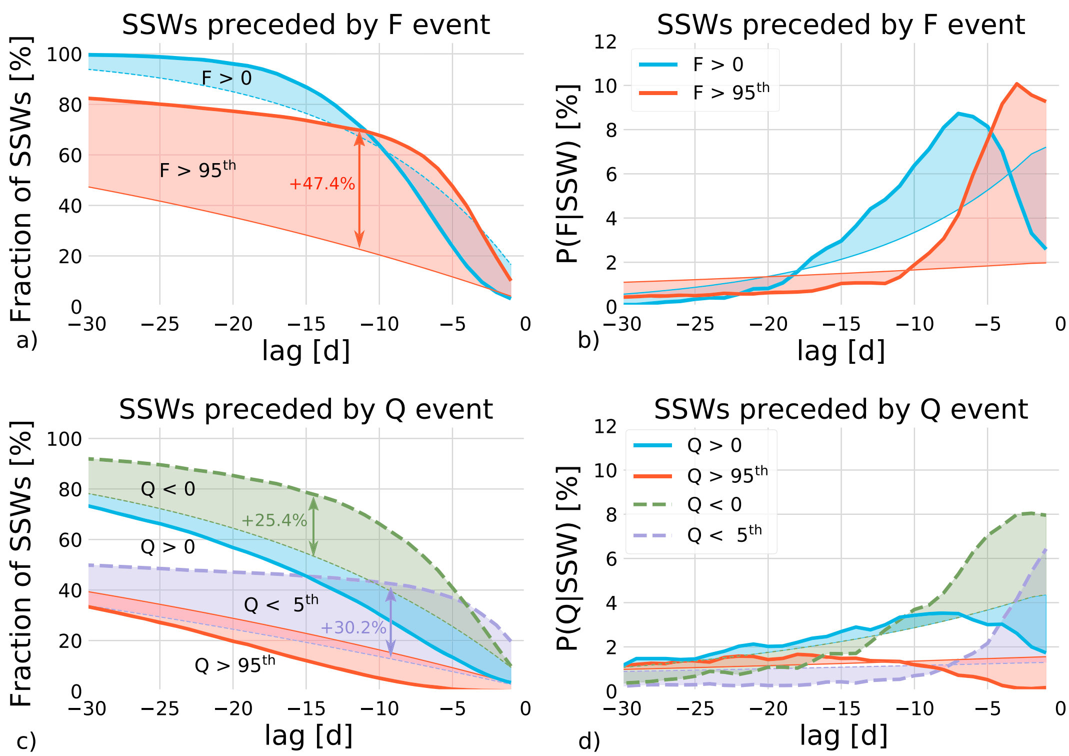

Figure 2. (a) Cumulative fraction of SSWs which are preceded by a $F_z > 0$ (blue) or $F_z > 95$th percentile event (red), as a function of lag before onset (which increases from right to left). (b) Daily probability of event occurrence prior to onset, which is the slope of the cumulative fraction. (c, d) Same but for $q_\phi \lessgtr 0$, $q_\phi < 5$th and $q_\phi > 95$th percentiles. The thin lines are computed from equation (6). SSW = stratospheric sudden warming event.

placeholder for either SSW or event E, we compute the probability of one or more events X happening within n days (irrespective of any other event or SSW occurring within the same time period) as

$$\mathcal{P}(X)(n) = 1 - \prod_{i=1}^{n} \left(1 - \overline{P(X)}(i)\right). \tag{6}$$

3. SSW Precursors

As described in section 1, both the *strength* and the *location* of EP wave breaking is important. For planetary Rossby waves, the meridional PV gradient represents the dynamical part of the refractive index (Albers & Birner, 2014). Therefore, we consider here the upward EP flux in the lower stratosphere (100 hPa) as the source for dynamical perturbations and the stratospheric meridional PV gradient (at 30 hPa) as the determining quantity for the propagation (and breaking) of those perturbations.

In order to verify that our experiments reproduce previous findings, we composite the evolution of F_z and q_ϕ in anomalous and standardized form in Figure 1. The upward wave activity does not significantly deviate from its climatological distribution (both mean and standard deviation) more than about 3 weeks before onset (transparent shading in Figure 1a) but strongly peaks during the week before the onset. The Probability Distribution Function (PDFs) in Figure 1b neatly show how the distribution just before the onset is distinct from the PDF including all days.

Figure 1c shows that the composite PV gradient is positive from about 10–70 days prior to onset, and the PDFs in Figure 1d are also different between pre-SSW days and all simulation days. Evidently, the signal is weaker for q_ϕ than for F_z, but in contrast to the latter, the composite evolution of q_ϕ differs significantly from the climatological distribution for lags of 90 days and more: Although the mean returns to 0, the 5th percentile remains significantly below the climatological 5th percentile.

Rather than relying on composites and mean evolution, we next quantify the fraction of SSWs which are preceded by anomalous upward EP flux and meridional PV gradient. We define the 5th and 95th percentiles as event thresholds, which are -1.77σ and 1.47σ for F_z and -1.67σ and 1.60σ for q_ϕ.

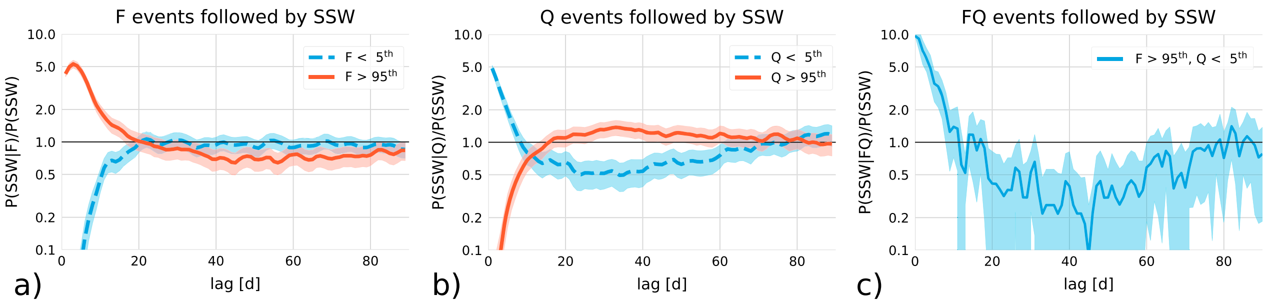

Figure 3. Conditional SSW probabilities, normalized to climatological SSW probability $\overline{P(SSW)} = 0.49\%$. (a) $P(SSW|F)$, that is, SSW probability given large positive (negative) F_z anomaly at lag 0 in red (blue). (b) $P(SSW|Q)$, that is, SSW probability given large positive (negative) q_ϕ anomaly at lag 0 in red (blue). (c) $P(SSW|FQ)$, that is, SSW probability given large positive F_z anomaly at lag 0 concurrent with large positive (negative) q_z anomaly in red (blue). All conditional probabilities converge toward $\overline{P(SSW)}$ (unity in the plots). Colored shading shows $\pm 2\sigma$ from the mean obtained from a 10,000-member bootstrap estimate. SSW = stratospheric sudden warming event.

Figures 2a and 2c show the fraction of SSWs in the data set which are preceded by at least one event (thick lines) as a function of lag before onset. Lag increases from right to left. The fractions are compared to the values we would expect if the events and SSWs were independent and are estimated from climatology using equations (5) and (6). The shaded area is the difference between the independent and the observed values.

Figures 2b and 2d show the slopes of the SSW fractions shown on the left to demonstrate at which lags most of the increase/decrease happens. We emphasize that an *event* here means the first crossing of a given threshold: If, for instance, the upward EP flux goes beyond the 95th percentile 5 days prior to onset and remains above the threshold until onset, the corresponding event of $F_z > 95$th will only be triggered at lag -5, and no event is detected at shorter lags. Similarly, on any given day, $P(F_z > 0)$ will be much lower than 50%. This is why, for example, the thick blue line of observed SSW fraction in Figure 2a is below the thin line at short lags and the thin blue line based on the climatological occurrence of F_z events in Figure 2b does not start at 50% but at 7.5%, even though about 50% of all individual days have $F_z > 0$. Figure 2b shows that $F_z > 0$ events have a higher probability of occurrence than if they were independent of SSWs between about lags -18 and -4, with a peak around 1 week before onset (thick blue line). At short lags, the fraction of SSWs preceded by an $F_z > 0$ event is lower than if F_z and SSWs were independent (Figure 2a, blue line) but becomes larger around lag -9 when going toward higher negative lags (toward the left) and remains higher at longer negative lags. Higher threshold events of $F_z > 95$th percentile happen more often than if they were independent of SSWs from about lag -11 all the way to onset, with a peak around lag -3 (Figure 2b, red line). Both the red and blue lines are below the independent (climatological) thin lines at higher lags. The resulting fraction of SSWs associated with such an event is always considerably higher than the same quantity assuming independence (red shaded area in Figure 2a), with a maximum difference of 47.4% around lag -12. This is because upward EP flux starts to strengthen about 2 to 3 weeks prior to onset and becomes steadily stronger as we move closer to the SSW, which means it will trigger a $F_z > 0$ event first and a $F_z > 95$th percentile event closer to onset, just like depicted in Figure 2b.

Looking at Figures 2c and 2d, the evolution of anomalously negative q_ϕ is similar to $F_z > 0$, with $q_\phi < 0$ events becoming more numerous than expected from independence at about lag -13 and $q_\phi < 5$th percentile events doing the same around lag -8 (green and purple dashed lines in Figure 2d). For positive q_ϕ events, the evolution is mirrored: The fraction of SSWs for both $q_\phi > 0$ and $q_\phi > 95$th percentile is lower than climatology (i.e., assuming independence of q_ϕ) at short lags (Figure 2c, blue and red), and the daily event probabilities change from lower to higher than expected from climatology with increasing lag before onset (Figure 2d, blue and red). Both curves remain above the daily probabilities estimated from climatology at long lags. The fraction of SSWs with negative PV gradient events is much larger than the climatological estimates (Figure 2c, green and purple), with maximum differences of 25.4% at lag -14 and 30.2% at lag -9, respectively.

The positive PV gradient events are associated with a slightly smaller SSW fraction at short lags, which converges back to the climatological value at longer lags and eventually becomes slightly higher at very long lags (not shown). Particularly from the daily event probabilities, we conclude that positive q_ϕ events, and therefore steeper meridional PV gradients, are associated with future SSWs at large lags and that weaker meridional PV gradients are associated with future SSWs at lags shorter than 2 weeks.

4. Conditional SSW Probabilities

We now use the results from the previous section to construct predictors for SSWs. That is, we invert the usual compositing or life cycle approach and detect instead single F_z and q_ϕ events. Then, we compute the probability of an SSW in the future, given an F_z or q_ϕ event happened (conditional probability). We will concentrate on the 5th and 95th percentile thresholds and from now on refer to them as *negative* and *positive* thresholds.

The important quantity to compute is the conditional probability $P(SSW|E)$, that is, the probability of a future SSW, given that a predefined event E has been detected. To investigate the potential for seasonal prediction, we will consider a future time range of up to 90 days. Figure 3 shows $P(SSW|E)$ for different events E, normalized to $\overline{P(SSW)}$. Note that all values converge toward unity at long lags, which means that P(SSW|E) → $\overline{P(SSW)}$. It is also clear that at long lags events E and SSWs must be independent, meaning that $P(SSW|E) \to P(SSW)$. Therefore, the empirically determined probability $P(SSW)$ equals $\overline{P(SSW)}$ as defined by equation (5), which validates our approach to compare against $\overline{P(SSW)}$ as outlined in section 1.

4.1. Upward EP Fluxes

Figure 3a shows $P(SSW|F)$ as a function of lag, that is, the probability of detecting an SSW x days in the future (lag > 0), given that we have detected a F event today (lag 0). The daily probability (i.e., the probability of occurrence at each individual lag) is given by Figure 3d. The red (blue) line shows the probabilities for the positive (negative) threshold, and the black line the climatological value $\overline{P(SSW)}$.

There is a large gain in information after the occurrence of a strong upward EP flux event (Figure 3a, red line), with the biggest increase in SSW probability (factor of 5) during the first week after the event. $P(SSW|F)$ is significantly larger than $\overline{P(SSW)}$ for just over 2 weeks, and there is a slightly (but statistically significant) lower SSW probability from about 5 weeks onward. About 20% of all positive F_z events are followed by an SSW within 2 weeks (computed using equation (6), not shown). For the negative F_z threshold (blue dashed line in Figure 1a), $P(SSW|F)$ is more than an order of magnitude smaller than $\overline{P(SSW)}$ for about a week and converges toward $\overline{P(SSW)}$ around the same time that the positive threshold does (around 20 days). Only 2% of all negative F_z events are followed by an SSW within 2 weeks (not shown). In contrast to the positive threshold, the negative threshold in F_z has no influence on SSW probability for lags beyond 3 weeks. To summarize, the power of prediction of F_z is greatest during the first week, decreases rapidly up to about 20 days, and it does not contribute to increased prediction skill beyond 4 weeks.

4.2. PV Gradient

Similar to a negative F_z event, the SSW probability decreases by an order of magnitude within the first week after a positive PV gradient event (Figure 3b, red line) and crosses the $\overline{P(SSW)}$ mark around 2 weeks after the event. Then, $P(SSW|Q)$ becomes slightly larger than $\overline{P(SSW)}$ between 4 and 5 weeks after the event.

Negative PV gradients (blue dashed) are similar in effect to positive F_z at short lags, as they increase the immediate SSW probability up to fivefold within the first week. However, in contrast to F_z, the SSW probabilities are lower than $\overline{P(SSW)}$ starting from the second week up to about 2 months. Three to 5 weeks after a negative q_ϕ event, the SSW probability is halved compared to $\overline{P(SSW)}$. Beyond 2 months, $P(SSW|Q)$ converges back to $\overline{P(SSW)}$. About 12% (3%) of all negative (positive) q_ϕ events are followed by an SSW within 2 weeks (not shown).

Thus, to summarize our results so far, for the short term, the use of F_z as a predictor for an SSW occurrence is powerful but yields little useful information beyond 3 weeks. Depending on the sign of the q_ϕ threshold, the meridional PV gradient is just as good a predictor as F_z in the short term. But it adds significant information at long lags, as for example, $P(SSW|Q)$ is statistically significantly lower (up to a factor of 2) than $\overline{P(SSW)}$ 15–60 days into the future.

4.3. Combined Probabilities

Following the dynamical idea that the PV gradient influences the orientation of EP fluxes, and that the PV gradient can therefore make the same EP flux more or less *efficient* in driving SSWs, we now consider the union of both events. That is, we compute $P(SSW|F \cap Q)$, the probability of a SSW happening within a certain time lag after upward EP flux crosses a specified threshold (F event) and the meridional PV gradient is larger (weaker) than a given positive (negative) threshold (Q event; Figure 3c).

There are now four possible combinations between the thresholds used in Figures 3a and 3b. However, as the negative F_z threshold corresponds to strongly decreased EP flux, there is no wave activity to be redirected by the PV gradient. Also, the positive F_z and q_ϕ events have opposing effects on the SSW probability (Figures 3a and 3b). Therefore, we only show the probabilities for the combination of the positive F_z and the negative q_ϕ thresholds in Figure 3c.

At short lags (~first week), the combination of the two precursors about doubles the SSW probability compared to each precursor individually, and it is now a full order of magnitude larger than the climatological value. Computing the cumulative probabilities for the first week (7 days, equation (6)), we get an ~6 times higher probability of any SSW happening within that period if we use the precursors (19% vs. 3.3%, not shown).

At long lags (~20–60 days), $P(SSW|F \cap Q)$ is 2–5 times smaller than climatology. In other words, the occurrence of SSWs is strongly reduced 20–60 days after a $F \cap Q$ event. In general, $P(SSW|F \cap Q)$ follows the $P(SSW|Q < 0)$ case (blue dashed line in Figure 3b), but the increase and decrease in SSW probability is more pronounced. The (cumulative) probability of an SSW occurring within this time period is about 3 times lower (6.2% vs. 17.3%, not shown) if we use the information from the precursors.

5. Conclusions

This study quantifies the probability of SSW occurrence as a function of two dynamical precursors. Based on earlier theoretical work, we define the precursor events as the crossing of thresholds of (a) anomalous upward EP flux at 100 hPa (F_z) and (b) anomalous stratospheric meridional PV gradient at 30 hPa (q_ϕ). Then, we show how the future occurrence of SSWs is statistically impacted by these events.

We find that F_z yields additional information for lead times of up to 3 weeks, whereas q_ϕ impacts the probability of SSW occurrence for both short and long lead times: Anomalously weak PV gradients favor SSW occurrence for about 1 week and make them less probable from 1 week to 2 months ahead. Anomalously strong PV gradients predict very low SSW probabilities for about 2 weeks but slightly increased SSW probability for all longer lead times, including the seasonal time scale.

Combining F_z and q_ϕ amplifies both the short- and long-term SSW probability signal. For instance, the probability of an SSW occurring the day after F_z crosses the 95th percentile (1.75σ) while q_ϕ is below the 5th percentile (-1.67σ) is an order of magnitude higher than the probability based on climatology (Figure 3c). This translates into a 19% chance of an SSW occurring within the first 7 days, compared to 3.3% within the same time period if we do not use the two precursors (as computed using equation (6)). It is interesting to note that the ~10-day window of increased SSW probability is similar to the current limit of dynamical forecasting models to predict SSWs (Karpechko, 2018; Tripathi et al., 2015, 2016). However, and perhaps more importantly, our method can also give useful guidance on much longer time scales: The SSW probability is significantly reduced compared to the independent estimate from climatology 20–60 days after the above events are detected. Whereas the independent estimate is ~17% for this time period, it is reduced to 6% when using the information from the precursors. Finally, we note that the above cited numbers depend on the exact threshold choices and lead times and are also reported as seasonal averages: Any different combination of these parameters would yield different numbers, but the overall conclusions would remain the same. We emphasize that this study is the first to attempt statistical SSW prediction based on dynamical arguments. We also note that one could explore other predictors or combinations thereof, but this is subject to a more comprehensive study which we leave for future work.

Acknowledgments
T. R. acknowledges support from NSF grant 1446292. M. J. acknowledges support from the Australian Research Council (ARC) Centre of Excellence for Climate System Science (CE110001028), and ARC grant FL150100035 during the revision of this manuscript. This work used the xarray (Hoyer & Hamman, 2017), parmap [https://github.com/zeehio/parmap], and aostools (Jucker, 2018) packages. We thank Eve Slavich from UNSW Stats Central for statistical support. We also acknowledge the Center for High Performance Computing at the University of Utah and the National Computational Infrastructure in Canberra for providing compute infrastructure and computing time. All analyzed data and the analysis script are published online (Jucker & Reichler, 2018).

References

Albers, J. R., & Birner, T. (2014). Vortex preconditioning due to planetary and gravity waves prior to sudden stratospheric warmings. *Journal of the Atmospheric Sciences*, *71*(11), 4028–4054. https://doi.org/10.1175/JAS-D-14-0026.1

Andrews, D. G., Holton, J. R., & Leovy, C. B. (1987). *Middle Atmosphere Dynamics, International geophysics series*. San Diego, CA: Academic Press.

Ayarzagüena, B., Langematz, U., & Serrano, E. (2011). Tropospheric forcing of the stratosphere: A comparative study of the two different major stratospheric warmings in 2009 and 2010. *Journal of Geophysical Research*, *116*, D18114. https://doi.org/10.1029/2010JD015023

Baldwin, M. P., & Dunkerton, T. J. (2001). Stratospheric harbingers of anomalous weather regimes. *Science*, *294*(5542), 581–4. https://doi.org/10.1126/science.1063315

Bancalá, S., Krüger, K., & Giorgetta, M. (2012). The preconditioning of major sudden stratospheric warmings. *Journal of Geophysical Research*, *117*, D04101. https://doi.org/10.1029/2011JD016769

Birner, T., & Albers, J. R. (2017). Sudden stratospheric warmings and anomalous upward wave activity flux. *Sola*, *13A*(Special_Edition), 8–12. https://doi.org/10.2151/sola.13A-002

Butchart, N., Clough, S. A., Palmer, T. N., & Trevelyan, P. J. (1982). Simulations of an observed stratospheric warming with quasigeostrophic refractive index as a model diagnostic. *Quarterly Journal of the Royal Meteorological Society*, *108*(457), 475–502. https://doi.org/10.1002/qj.49710845702

Butler, A. H., Seidel, D. J., Hardiman, S. C., Butchart, N., Birner, T., & Match, A. (2015). Defining sudden stratospheric warmings. *Bulletin of the American Meteorological Society*, *96*(2), 150904101253006. https://doi.org/10.1175/BAMS-D-13-00173.1

Charlton, A. J., & Polvani, L. M. (2007). A new look at stratospheric sudden warmings. Part I: Climatology and modeling benchmarks. *Journal of Climate*, *20*(3), 449–469. https://doi.org/10.1175/JCLI3996.1

Charlton, A. J., Polvani, L. M., Perlwitz, J., Sassi, F., Manzini, E., Shibata, K., et al. (2007). A new look at stratospheric sudden warmings. Part II: Evaluation of numerical model simulations. *Journal of Climate*, *20*(3), 470–488. https://doi.org/10.1175/JCLI3994.1

Charney, J., & Drazin, P. (1961). Propagation of planetary-scale disturbances from the lower into the upper atmosphere. *Journal of Geophysical Research*, *66*, 83–109.

Dickinson, R. E. (1969). Vertical propagation of planetary Rossby waves through an atmosphere with Newtonian cooling. *Journal of Geophysical Research*, *74*(4), 929–938.

Dunn-Sigouin, E., & Shaw, T. A. (2015). Comparing and contrasting extreme stratospheric events, including their coupling to the tropospheric circulation. *Journal of Geophysical Research: Atmospheres*, *120*, 1374–1390. https://doi.org/10.1002/2014JD022116

Eliassen, A., & Palm, T. (1961). On the transfer of energy in stationary mountain waves. *Geofysiske publikationer*, *22*(3), 1–23.

Esler, J. G., & Matthewman, N. J. (2011). Stratospheric sudden warmings as self-tuning resonances. Part II: Vortex displacement events. *Journal of the Atmospheric Sciences*, *68*, 2505–2523.

Garfinkel, C. I., Hartmann, D. L., & Sassi, F. (2010). Tropospheric precursors of anomalous Northern Hemisphere stratospheric polar vortices. *Journal of Climate*, *23*(12), 3282–3299.

Holton, J. R. (1974). Forcing of mean flows by stationary waves. *Journal of the Atmospheric Sciences*, *31*(4), 942–945. https://doi.org/10.1175/1520-0469(1974)031<0942:FOMFBS>2.0.CO;2

Horan, M. F., & Reichler, T. (2017). Modeling seasonal sudden stratospheric warming climatology based on polar vortex statistics. *Journal of Climate*, *30*(24), 10,101–10,116. https://doi.org/10.1175/JCLI-D-17-0257.1

Hoyer, S., & Hamman, J. J. (2017). xarray: N-D labeled arrays and datasets in Python. *Journal of Open Research Software*, *5*, 1–6. https://doi.org/10.5334/jors.148

Jucker, M. (2016). Are sudden stratospheric warmings generic? Insights from an idealized GCM. *Journal of the Atmospheric Sciences*, *73*(12), 5061–5080. https://doi.org/10.1175/JAS-D-15-0353.1

Jucker, M. (2018). mjucker/aostools: aostools v2.1.5. https://doi.org/10.5281/ZENODO.1252733

Jucker, M., & Reichler, T. (2018). Analysis for "Dynamical precursors for statistical prediction of stratospheric sudden warming events". https://doi.org/10.17632/ffhv8kn7m5.2

Karoly, D. J., & Hoskins, B. J. (1982). Three dimensional propagation of planetary waves. *Journal of the Meteorological Society of Japan. Ser. II*, *60*(1), 109–123. https://doi.org/10.2151/jmsj1965.60.1_109

Karpechko, A. Y. (2018). Predictability of sudden stratospheric warmings in the ECMWF extended range forecast system. *Monthly Weather Review*, *146*, 17–0317. https://doi.org/10.1175/MWR-D-17-0317.1

Labitzke, K. (1977). Interannual variability of the winter stratosphere in the Northern Hemisphere. *Monthly Weather Review*, *105*, 762–770. https://doi.org/10.1175/1520-0493(1977)105<0762:IVOTWS>2.0.CO;2

Labitzke, K. (1981). Stratospheric-mesospheric midwinter disturbances: A summary of observed characteristics. *Journal of Geophysical Research*, *86*(C10), 9665. https://doi.org/10.1029/JC086iC10p09665

Limpasuvan, V., Thompson, D. W. J., & Hartmann, D. L. (2004). The life cycle of the Northern Hemisphere sudden stratospheric warmings. *Journal of Climate*, *17*(13), 2584–2596. https://doi.org/10.1175/1520-0442(2004)017<2584:TLCOTN>2.0.CO;2

Martineau, P., & Son, S.-W. (2015). Onset of circulation anomalies during stratospheric vortex weakening events: The role of planetary-scale waves. *Journal of Climate*, *28*(18), 7347–7370. https://doi.org/10.1175/JCLI-D-14-00478.1

Matsuno, T. (1970). Vertical propagation of stationary planetary waves in the winter Northern Hemisphere. *Journal of the Atmospheric Sciences*, *27*(6), 871–883. https://doi.org/10.1175/1520-0469(1970)027<0871:VPOSPW>2.0.CO;2

Matsuno, T. (1971). A dynamical model of the stratospheric sudden warming. *Journal of the Atmospheric Sciences*, *28*(8), 1479–1494. https://doi.org/10.1175/1520-0469(1971)028<1479:ADMOTS>2.0.CO;2

Matthewman, N. J., & Esler, J. G. (2011). Stratospheric sudden warmings as self-tuning resonances. Part I: Vortex splitting events. *Journal of the Atmospheric Sciences*, *68*(11), 2481–2504.

McIntyre, M. E. (1982). How well do we understand the dynamics of stratospheric warmings? *Journal of the Meteorological Society of Japan*, *60*(1), 37–65.

Nakagawa, K. I., & Yamazaki, K. (2006). What kind of stratospheric sudden warming propagates to the troposphere? *Geophysical Research Letters*, *33*, L04801. https://doi.org/10.1029/2005GL024784

Nishii, K., Nakamura, H., & Miyasaka, T. (2009). Modulations in the planetary wave field induced by upward-propagating Rossby wave packets prior to stratospheric sudden warming events: A case-study. *Quarterly Journal of the Royal Meteorological Society*, *135*(638), 39–52. https://doi.org/10.1002/qj.359

Palmeiro, F. M., Barriopedro, D., García-Herrera, R., & Calvo, N. (2015). Comparing sudden stratospheric warming definitions in reanalysis data*. *Journal of Climate*, *28*(17), 6823–6840. https://doi.org/10.1175/JCLI-D-15-0004.1

Palmer, T. N. (1981). Aspects of stratospheric sudden warmings studied from a transformed Eulerian-mean viewpoint. *Journal of Geophysical Research*, *86*(C10), 9679. https://doi.org/10.1029/JC086iC10p09679

Polvani, L. M., & Waugh, D. W. (2004). Upward wave activity flux as a precursor to extreme stratospheric events and subsequent anomalous surface weather regimes. *Journal of Climate*, *17*(18), 3548–3554. https://doi.org/10.1175/1520-0442(2004)017<3548:UWAFAA>2.0.CO;2

Reichler, T., & Kim, J. (2008). How well do coupled models simulate today's climate? *Bulletin of the American Meteorological Society*, *89*(3), 303–312. https://doi.org/10.1175/BAMS-89-3-303

Scaife, A. A., Comer, R. E., Dunstone, N. J., Knight, J. R., Smith, D. M., MacLachlan, C., et al. (2017). Tropical rainfall, Rossby waves and regional winter climate predictions. *Quarterly Journal of the Royal Meteorological Society*, *143*(702), 1–11.

Schneidereit, A., Peters, D. H. W., Grams, C. M., Quinting, J. F., Keller, J. H., Wolf, G., et al. (2017). Enhanced tropospheric wave forcing of two anticyclones in the prephase of the January 2009 major stratospheric sudden warming event. *Monthly Weather Review*, *145*(5), 1797–1815. https://doi.org/10.1175/MWR-D-16-0242.1

Schoeberl, M. R. (1978). Stratospheric warmings: Observations and theory. *Reviews of Geophysics*, *16*(4), 521–538. https://doi.org/10.1029/RG016i004p00521

Scott, R. K., & Polvani, L. M. (2004). Stratospheric control of upward wave flux near the tropopause. *Geophysical Research Letters*, *31*, L02115. https://doi.org/10.1029/2003GL017965

Scott, R. K., & Polvani, L. M. (2006). Internal variability of the winter stratosphere. Part I: Time-independent forcing. *Journal of the Atmospheric Sciences*, *63*(11), 2758–2776. https://doi.org/10.1175/JAS3797.1

Shaw, T. A., Perlwitz, J., & Weiner, O. (2014). Troposphere-stratosphere coupling: Links to North Atlantic weather and climate, including their representation in CMIP5 models. *Journal of Geophysical Research: Atmospheres*, *119*, 5864–5880. https://doi.org/10.1002/2013JD021191

Sigmond, M., Scinocca, J. F., Kharin, V. V., & Shepherd, T. G. (2013). Enhanced seasonal forecast skill following stratospheric sudden warmings. *Nature Geoscience*, *6*(2), 98–102. https://doi.org/10.1038/ngeo1698

Simpson, I. R., Blackburn, M., & Haigh, J. D. (2009). The role of eddies in driving the tropospheric response to stratospheric heating perturbations. *Journal of the Atmospheric Sciences*, *66*(5), 1347–1365. https://doi.org/10.1175/2008JAS2758.1

Tripathi, O. P., Baldwin, M., Charlton-Perez, A., Charron, M., Cheung, J. C. H., Eckermann, S. D., et al. (2016). Examining the predictability of the stratospheric sudden warming of January 2013 using multiple NWP systems. *Monthly Weather Review*, *144*(5), 1935–1960. https://doi.org/10.1175/MWR-D-15-0010.1

Tripathi, O. P., Baldwin, M., Charlton-Perez, A., Charron, M., Eckermann, S. D., Gerber, E., et al. (2015). The predictability of the extratropical stratosphere on monthly time-scales and its impact on the skill of tropospheric forecasts. *Quarterly Journal of the Royal Meteorological Society*, *141*(689), 987–1003.